Dynamics of hypersaline coastal waters in the Great Barrier Reef

FERNANDO P. ANDUTTA[1, 2, *], PETER V. RIDD[1], ERIC WOLANSKI[2]

[1] School of Engineering and Physical sciences, James Cook University, Townsville QLD 4811, Australia.
[2] ACTFR, James Cook University, Townsville, QLD, 4811, and Australian Institute of Marine Science, Townsville, Australia.

[*] Corresponding author. Email: fernando.andutta@jcu.edu.au

ABSTRACT

The coastal waters of the Great Barrier Reef (GBR) are hypersaline (salinity ~37) during the dry season as a result of evaporation greatly exceeding rainfall, of shallow waters, and of the presence of numerous bays along the coast preventing rapid flushing. These hypersaline waters are not flushed out by salinity-driven baroclinic currents because these waters are vertically well-mixed. Instead these waters are transported by a longshore residual current and thus form a coastal boundary layer of hypersaline waters. As a result the hypersalinity distribution is 2-D with both cross-shelf and longshore gradients of salinity. The cross-shelf gradients are largely controlled by turbulent diffusion, while the longshore gradients are controlled by the residual currents that transport hypersaline waters longshore south ward in the central and southern regions of the GBR. Because every bay supplies hypersaline waters, the width of the coastal hypersaline layer increases southwards. Steady state is reached in about 100 days, which is the typical duration of the dry season. The dynamics of the GBR hypersaline coastal boundary layer thus differ from the classical inverse hypersaline systems, e.g. in Saloum River Estuary, Laguna San Ignacio, Mission Bay, Tomales Bay, San Diego Bay, Hervey Bay, Shark Bay, Coorong Coast Lagoon, Spencer Gulf, Gulf of California and many others where the salinity gradient is mainly 1-D with a dominant along-channel salinity gradient.

Keywords: Salinity, evaporation, diffusion, trapping, diffusion-advection balance.

1. Introduction

Hypersaline systems are bodies of water such as estuaries, bays and gulfs with salinity larger than that of the oceanic waters ca. 35.5 (psu). The occurrence of hypersaline waters in estuaries, bays and coastal waters is caused by the excess of evaporation over freshwater input from rainfall and rivers. In such systems, the salinity does not continue to increase indefinitely even though evaporation continues as excess salt is flushed to the ocean by the water circulation (Lennon et al., 1987). Hypersalinity may occur in systems of a wide range of scales, typically from scales of 10's of km such as the estuaries in tropical and sub-tropical Australia, 100's of km such as in Spencer Gulf, the Gulf of California and its lagoons, the Great Australian Bight and the Gulf of Kachchh in the Arabian Sea, and even 1000's of km such as in the Mediterranean Sea and the Red Sea (Phillips, 1966; Lacombe and Richez, 1982; Wolanski, 1986; Nunes Vaz et al., 1990; Bray and Rubles, 1991; Chadwick and Largier, 1999; Valle-Levinson et al., 2001; Gutierrez de Velasco and Winant, 2004; Ribbe, 2006; Vethamony et al., 2007). In most systems hypersalinity is a seasonal phenomenon occurring only in the dry season, but in some systems such as Baja California, Mexico, the hypersalinity may persist throughout the year. As salinity is a conservative tracer, it is possible to use advection-diffusion models to estimate water residence times from observations of hypersalinity (Wang et al., 2007). Such models are easiest to apply in 1-D situations when homogeneity can be assumed both vertically and cross-channel. Hypersalinity (salinity ~37), has been reported in coastal waters of the Great Barrier Reef (GBR; Fig. 1) but only during the dry season typically from July to November (Wolanski et al., 1981; Walker, 1981, 1982; Wolanski, 1994). The dynamics of these hypersaline waters are unknown. A closed analytical solution, such a 1-D model (i.e. with a salinity gradient occurring only cross-shelf) suggests that the width of the hypersaline coastal zone depends on the balance between evaporation and cross-shelf diffusion (Wang et al., 2007). Such 1-D models however ignore the patchiness of the hypersalinity distribution as well as the longshore gradients. In this paper we remove this disadvantage by using a 2-D, high resolution numerical model, verified against field data, to simulate their dynamics. A 2-D model was justified because the baroclinic circulation could safely be neglected as the waters are vertically well-mixed. We show that the dynamics of the GBR hypersaline waters differ from that in most other coastal hypersaline systems.

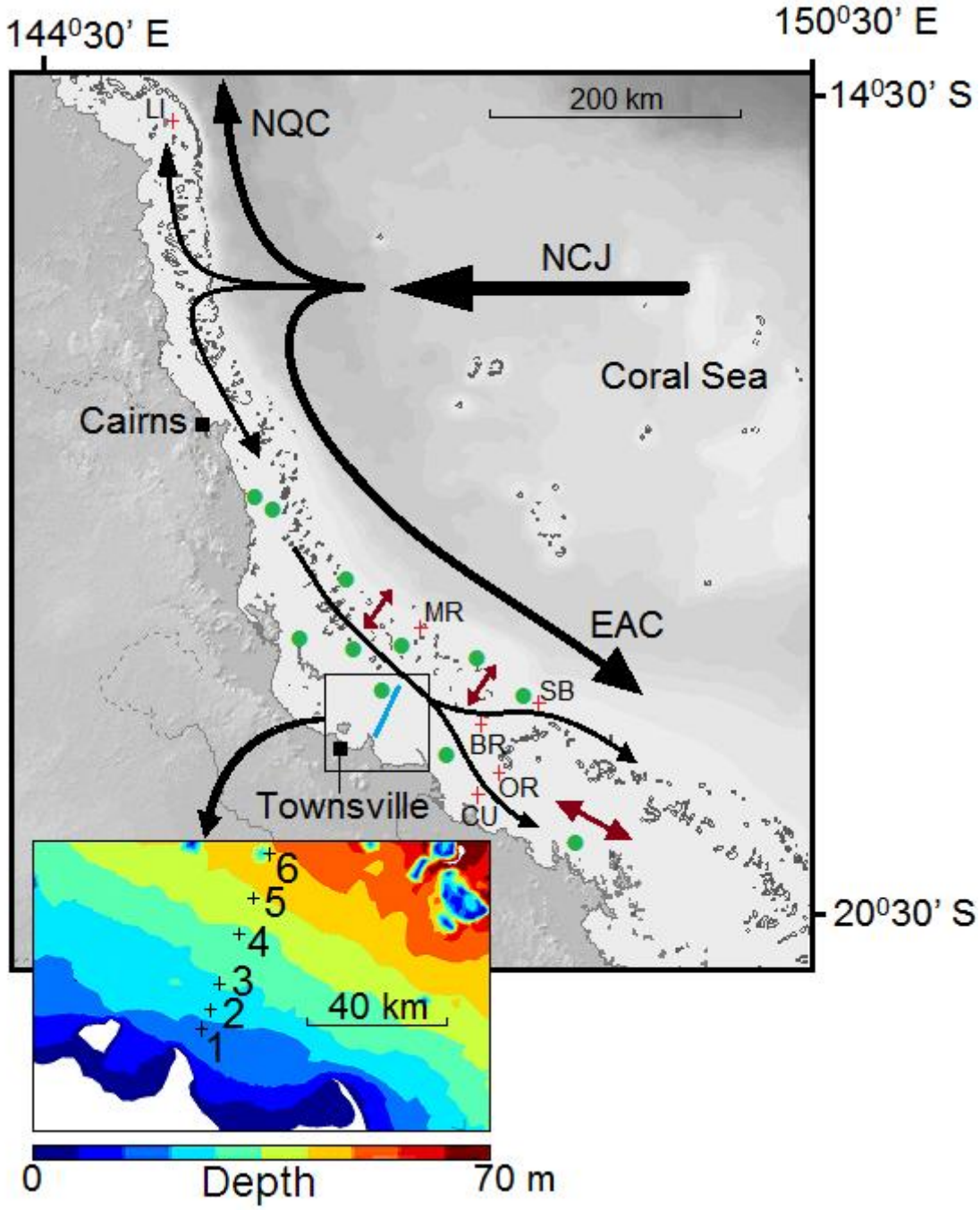

Figure 1 – Location map of the central section of the Great Barrier Reef (Queensland, Australia). Field data sites of tidal currents (•), residual currents (+) and the salinity sites (1-6) along the transect (blue line). Details of bathymetry and salinity sites are shown in the inset. NCJ= North Caledonia Jet; EAC = Eastern Australian Current; NQC = North Queensland Current. The residual currents are indicated by the black arrows. The dominant direction of the tidal currents is indicated by the double pointed brown arrows.

2. Methods

2.1 Field data

The field data on salinity in coastal waters in the dry season are those of Wolanski and Jones (1979) who measured salinity throughout the water column, at weekly intervals, throughout 1979, at six sites along a 58-km long cross-shelf transect shown in the inset of Fig. 1. There are only occasional measurements of salinity in the bays in the dry season, namely Walker (1981) for Cleveland Bay in 1978, Wolanski and Ridd (1990) and Sheaves (2006) for Bowling Green Bay in 1985.

Field data of currents (tidal and low-frequency) at six moored current meter sites and of tides at eleven sites were obtained from Andrews and Bode (1988), Andrews (1983), Wolanski and Pickard (1985), Wolanski et al. (1989), and Spagnol et al. (2001). The location of the current meter sites is shown in Fig. 1 and details of their location and references are listed in Table 1.

Table 1 – Comparison between observed and predicted alongshore residual currents (m s^{-1}) of six sites (+) shown in Fig. 1. Predicted residual currents for different inflows Q (Sv) of the Coral Sea. The root mean square error RMSE (m s^{-1}) is shown in the last row. The data sources *, ** and *** are respectively Andrews (1983), Wolanski et al. (1989), and Spagnol et al. (2001).

Residual currents in the GBR in m s^{-1}								
Site name	Latitude S	Longitude E	observed	Q = 0	Q = 2	Q = 4	Q = 6	Source
Lizard Island LI	14.7406	145.4253	0.05 (north)	0.00 (north)	0.06 (north)	0.07 (north)	0.10 (north)	***
Cape Upstart CU	19.6253	147.9142	0.11 (south)	0.01 (south)	0.06 (south)	0.10 (south)	0.10 (south)	***
Old Reef OR	19.4071	148.0197	0.10 (south)	0.01 (south)	0.05 (south)	0.09 (south)	0.11 (south)	**
near shelf break SB	18.8311	148.2896	0.25 (south)	0.01 (south)	0.10 (south)	0.20 (south)	0.28 (south)	*
Myrmidon Reef MR	18.2452	147.4100	0.18 (south)	0.01 (south)	0.16 (south)	0.25 (south)	0.31 (south)	*
Bowden Reef BR	19.0600	147.9597	0.1-0.25 (south)	0.00 (south)	0.02 (south)	0.02 (south)	0.03 (south)	**
RMSE	-	-	-	0.14	0.08	0.04	0.07	-

2.2 *Numerical model*

The GBR bathymetry is very complex with ~2800 reefs scattered over its 2600 km length, with individual reefs ranging in area from ~0.01 to ~100 km^2 and often separated by narrow passages. A high horizontal resolution is required because low resolution models erase the smaller reefs and do not yield the correct shear distribution near the edges of the remaining reefs; thus they do not simulate correctly the dispersive processes (Wolanski et al., 1996). It is an unresolved challenge to use finite-difference, regular grids models to model the whole GBR (King and Wolanski, 1996; Spagnol et al., 2001; Brinkman et al., 2002; Luick et al., 2007). To avoid these disadvantages we have thus used the non-structured grid model SLIM (Lambrechts et al., 2008). The cell size varied from 300m near reefs, headlands and islands and the coast to cells of several kilometers over the shelf far from reefs and the land (Fig. 2). We focused the study on the central and southern region of the GBR, thus explaining the high resolution of the grid in these areas. The bathymetry was derived from the data of Webster and Petkovic (2005) with a resolution of 250 m. The maximum depth was 200 m. The offshore open boundary conditions were the tides from TOPEX and the Coral Sea inflow Q (Fig. 2). This water inflow in the GBR from the adjoining Coral Sea is an unknown fraction of the North Caledonian Jet (NCJ; Fig. 1) (Andrews and Clegg, 1989; Ganachaud et al., 2007). The NCJ generates a southward net current (the East Australian Current) to the south of the separation point and a northward net current (the North Queensland Current, NQC) to the north of the separation point. This inflow is thus little known. It was considered an external parameter to be adjusted until the model predictions for the residual currents match well the observed currents. For the simulations we varied the Coral Sea inflow Q in the range 0–6 Sv (1 Sv = 10^6 m^3 s^{-1}).

For the wind stress, a temporally variable and spatially uniform wind field was taken from the data of Wolanski (1994) at the Rib Reef weather station (18°28’50’’ S, 146°52’12’’ E).

The evaporation rate was assumed to be 0.005 m d^{-1} following Wang et al. (2007). Its value may vary spatially and temporally depending upon air temperature and humidity, water temperature and wind but this variation is believed to be small in the study area (Wang et al., 2007). The bottom friction was parameterized using a quadratic expression (Lambrechts et al., 2008). The horizontal diffusion coefficient K_h applied to each grid cell was size dependent following Okubo (1971). Okubo’s formula applies for open-water and it under-estimates the true value of K_h in the presence of macro-turbulence generated by a complex bathymetry

(Wolanski et al., 1984; de Brauwere et al., 2011), thus a factor was used to increase mixing at the sub-grid scale. It resulted in:

$$K_h = f\,[2.05 \times 10^{-4} \times r^{1.15}] \qquad (1)$$

where r is the grid size and f is a factor that was set to 2, 20, and 200 in sensitivity analyses.

The initial salinity when starting the model in August was set at 35.5 following the observations of Wolanski and Jones (1979). In all the simulations the system was started at rest in August.

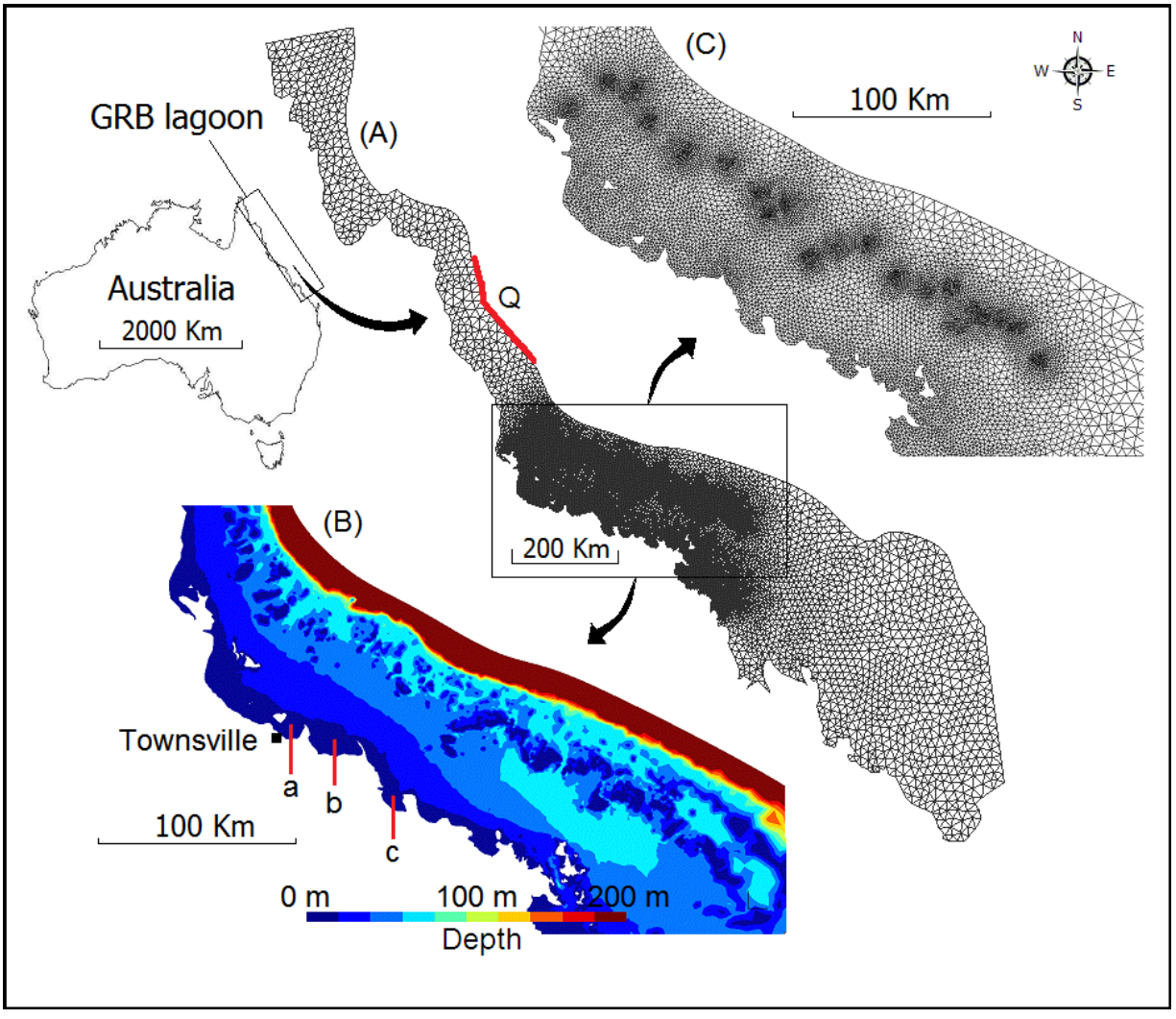

Figure 2 – (A) The numerical mesh of the whole GBR, (B) the bathymetry of the high resolution area, and (C) high resolution area of the numerical grid. Q denotes the location of

the Coral Sea inflow. a, b and c denote Cleveland Bay, Bowling Green Bay and Upstart Bay, respectively.

3. Results

For the simulation we varied (a) the values of Coral Sea inflow, (b) the horizontal diffusion coefficient K_h, and (c) the wind stress. The tidal currents are mainly cross-shelf in areas of low reef density and long-shelf in areas of high reef density; they are channeled between high reef density zones and the coast especially so offshore from Cape Upstart (Fig. 1; Church et al., 1985; Andrews and Bode, 1988; Wolanski, 1994; Spagnol et al., 2001; Lambrechts et al., 2008). Over 95% of the high frequency currents in the GBR lagoon is well represented by the semidiurnal tide components M_2, N_2, S_2 and K_2, and the diurnal components O_1, P_1, K_1 (Andrews and Bode,1988). The ellipses of the predicted tidal currents (not shown) agreed well with the observations of Andrews and Bode (1988).

Table 1 shows that the predicted residual currents assuming a Coral Sea inflow of 2 Sv are too small compared to the observations. For an inflow of 6 Sv, the predicted currents are too large. The best agreement in both magnitude and direction was obtained for an inflow of 4 Sv, with the Root Mean Square Error RMSE equal to 0.04 m s^{-1}.

The predicted circulation over the GBR continental shelf reproduces well the results of King and Wolanski (1996), Spagnol et al. (2001), Brinkman et al. (2002) and Luick et al. (2007), the main difference being that, in order to reproduce the observations, the inflow from the Coral Sea needs to be 4 Sv, i.e. twice as large as that previously assumed.

The data on the observed and predicted salinity in coastal waters along the cross-shelf transect are shown in Fig. 3. Fig. 3A shows temporal salinity changes at site 1 (inshore) for different values for the Coral Sea inflow in the range 0–6 Sv, and different values for the factor (f) from (Eq. (1)). From this figure it is apparent that an inflow of ~4–6 Sv is necessary for the model to reproduce the observations. The wind and tides also modulate the hypersalinity. In the absence to wind the model predicts spring-neap tidal fluctuations of the salinity inshore (Fig. 3B), with the peaks and troughs of the salinity corresponding to neap and spring conditions respectively. The effect of the tradewinds was to increase the salinity at the inshore sites while monsoonal winds decreased the salinity at the inshore sites (Fig. 3C). Table

2 shows that the salinity model best fits the salinity data (RMSE from the six sites w 0.1) for an inflow from the Coral Sea of inflow of 4 Sv and the factor f = 20 in Eq. (1).

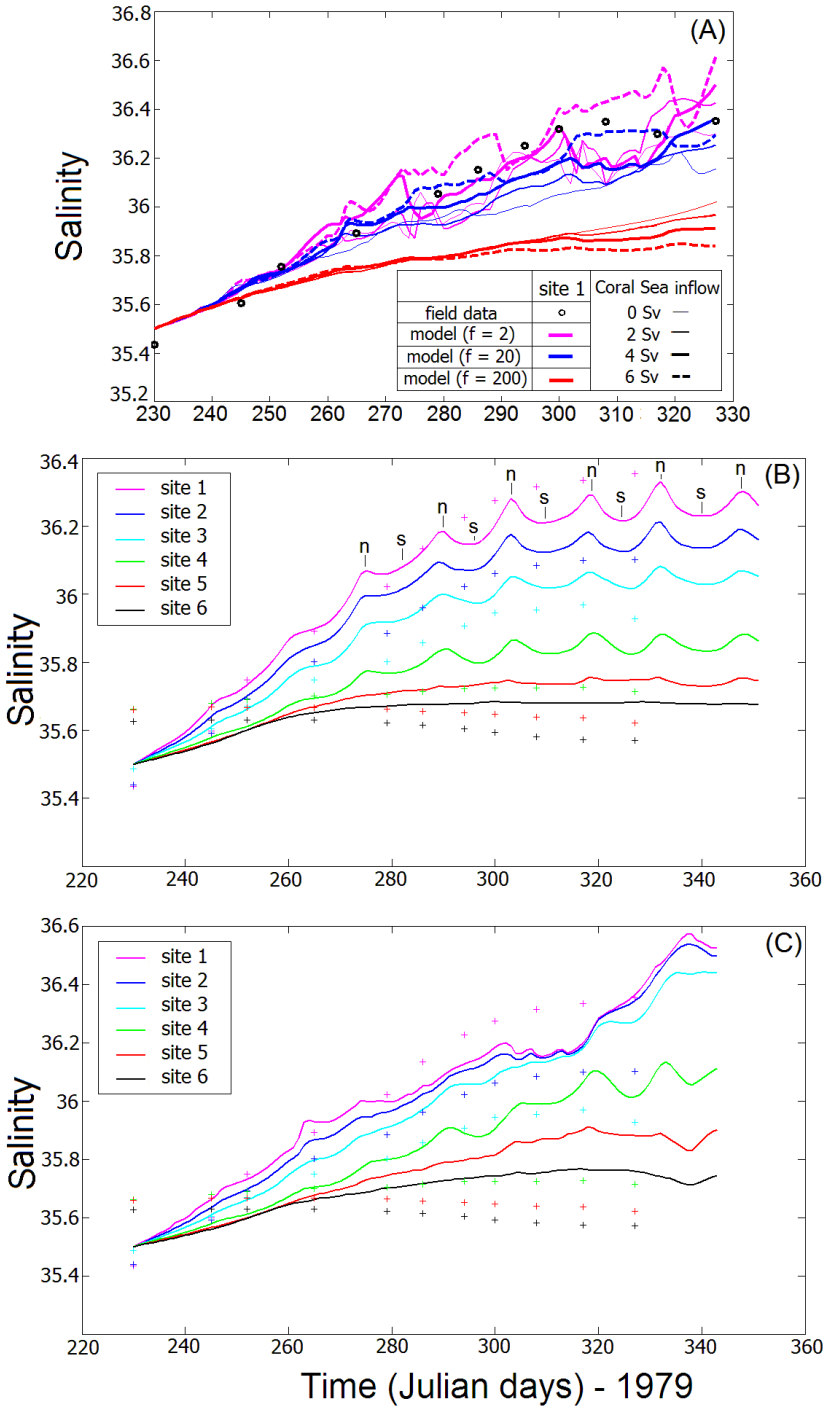

Figures 3 – Time series-plot of (A) the salinity (psu) at site 1 – inshore – as observed (year 1979) and predicted for different values of the Coral Sea inflow and the factor f in Eq. 1. (B) Observed and predicted salinity without wind at the six sites in the cross-shelf salinity

transect, where periods of neap tides (n) and spring tides (s) are indicated. (C) Observed (dots) and predicted (continuous lines) salinity with the variable wind stress.

Table 2 – The root mean square error RMSE of the salinity (psu) at sites 1 to 6 (Figure 1) for different inflows Q (Sv) of the Coral Sea, and the factor f in Eq. 1.

Site location								
		site 1	site 2	site 3	site 4	site 5	site 6	all sites
Distance from coast (km)		10	15	22	34	46	58	-
Latitude S		19.1521	19.1121	19.0530	18.9404	18.8590	18.7581	-
Longitude E		147.0874	147.1089	147.1375	147.1931	147.2337	147.2779	-
Root mean square error (psu) at sites 1 to 6								
Q	**f**	**site 1**	**site 2**	**site 3**	**site 4**	**site 5**	**site 6**	**all sites**
0	0	0.1947	0.1691	0.1565	0.1423	0.1693	0.1727	0.1674
0	20	0.1505	0.1148	0.1212	0.1502	0.1738	0.1477	0.1430
0	200	0.2888	0.1412	0.1708	0.1988	0.1911	0.1507	0.1902
2	0	0.1983	0.1797	0.1546	0.1650	0.1822	0.1844	0.1774
2	20	0.1274	0.1496	0.1647	0.1486	0.1638	0.1756	0.1550
2	200	0.2873	0.1403	0.1713	0.1943	0.1909	0.1912	0.1959
4	0	0.1158	0.1308	0.1549	0.1583	0.1410	0.1024	0.1339
4	20	0.0913	0.0883	0.1063	0.1322	0.1513	0.1207	0.1150
4	200	0.2621	0.1557	0.1285	0.1417	0.1870	0.1846	0.1766
6	0	0.1018	0.2001	0.1704	0.1895	0.1648	0.1498	0.1627
6	20	0.0994	0.0919	0.1431	0.1583	0.1584	0.1146	0.1276
6	200	0.3287	0.1842	0.1194	0.1621	0.1642	0.1558	0.1857

The predicted surface salinity maps of the Central Section of the Great Barrier lagoon are shown at steady state (100^{th} day of simulation) in Fig. 4A (with wind) and 4B (no wind). The predicted hypersalinity reaches a peak value of 2 and the width of the coastal boundary layer of hypersaline waters increases southwards from Cleveland Bay, to Bowling Green Bay to Upstart Bay.

The model performed well in predicting the hypersaline waters in the bays, namely about (36.0–36.6), (36.6–37.0) and (36.6–37.0) in Cleveland Bay, Bowling Green Bay and Upstart Bay respectively; these values agree with observations of Walker, (1981) and Sheaves (2006). The hypersaline waters were not predicted between the latitudes 15 S–17 S, which is the region where we have applied the Coral Sea inflow Q. This is in agreement with field results of Orr (1933), Brandon (1973) and Pickard (1977). It should also be noted that this region receives higher rainfall than the most of the GBR lagoon which may be the reason that no hypersaline water was measured.

The influence of the application of a southeasterly wind stress is to lower the salinity of bays (Fig. 4A) compared with conditions of no wind (Fig. 4B). For example, the maximum salinity in Bowling Green Bay and Upstart Bay is 36.5 when wind is considered rising to 36.8 with no wind. The simulation with wind (Fig. 4A) also shows hypersaline waters of up to 37 in a 100 km long coastal band from Cleveland Bay to Ingham, while for the simulation with no wind stress (Fig. 4B), the highly hypersaline water is confined to Cleveland Bay.

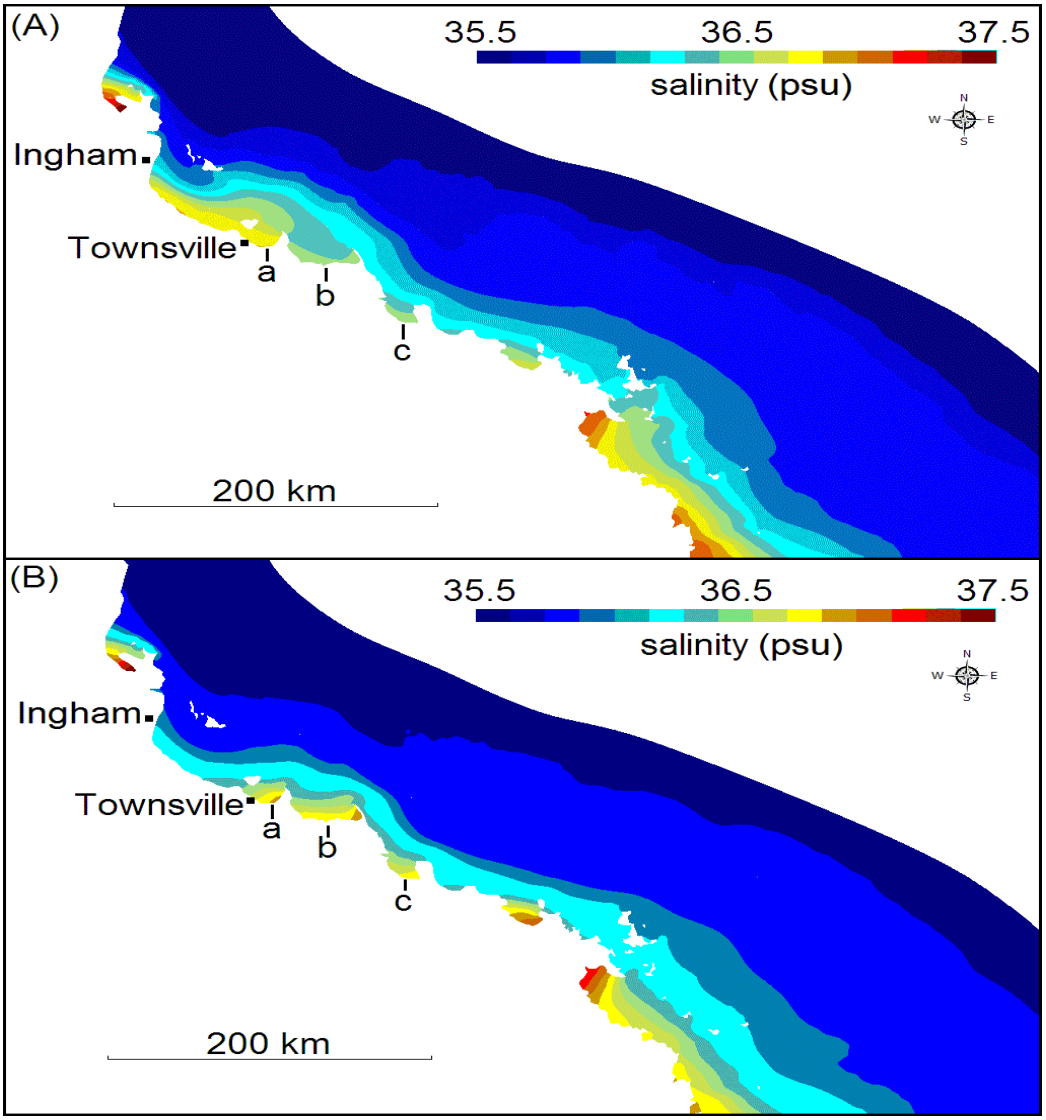

Figure 4 – Predicted salinity distribution at steady state (A) in the presence of the wind and (B) assuming no wind. a, b and c denote Cleveland Bay, Bowling Green Bay and Upstart Bay.

4. Discussion

The Coral Sea inflow determines the residual currents in the GBR. An inflow of 4 Sv is required to match the observations of residual currents on the GBR continental shelf. This residual circulation combined with tidal mixing determines the time it takes for steady state conditions to prevail. Using f = 20, steady state for salinity is achieved after 90 days, while for f = 2 it required more than 160 days. For f = 200 the steady-state condition was reached much faster (~ 70 days), however, the salinity at the inshore sites did not rise measurably and thus The Coral Sea inflow determines the residual currents in the lagoon. An inflow of 4 Sv is required to match the observations of residual currents on the GBR continental shelf. This residual circulation combined with tidal mixing determines the time it takes for steady state conditions to prevail. Using f = 20, a steady state for salinity is achieved after 90 days, while for f = 2 it required more than 160 days. For f = 200 the steady-state condition was reached much faster (~70 days), however, the salinity at the inshore sites did not increase measurably and thus did not reproduce the observations.

The results show that the GBR hypersaline zone exists in all wind conditions in the dry season. Hypersaline waters are generated every day and in every bay. Every bay is very shallow (mean depth <5 m) and drains extensive hypersaline salt flats; salinity in inshore waters of these bays at the mouth of tidal creeks peaks at 37.7 in Bowling Green Bay and 38.7 in Upstart Bay. The residual currents export hypersaline waters from bay to bay longshore southwards; as result the width of the hypersaline zone increases longshore southwards. At the same time, turbulent diffusion spreads the isohalines seawards. The combination of the residual southwards currents with the cross-shelf export of salinity from each bay and turbulent diffusion determines how the width of hypersaline zone increases longshore southwards.

The dynamics of the hypersaline coastal boundary layer in the GBR differs from that in other coastal hypersaline systems in Australia. In Hervey Bay and in Shark Bay (Fig. 5) that are relatively shallow systems (average depth <10 m), vertical mixing inhibits vertical stratification (Nahas et al., 2005; Ribbe, 2006). In those systems the hypersaline waters are trapped in the bay without the possibility of escaping sideways or along the bottom. Similarly, a salinity maximum zone develops in Australian tropical estuaries in the dry season (Wolanski, 1986). A similar long-term trapping of hypersaline waters has been reported for several estuaries and shallow bays world-wide, e.g. the Saloum River Estuary, Tomales Bay, Coorong Lagoon, Gulf of California and Laguna San Ignacio (Diop et al., 1997; Largier et al.,

1997; Lavin et al., 1998; Webster, 2010; Winant and de Velasco, in press). In contrast, in Spencer Gulf (Fig. 5), which is a deeper near the mouth (50 m), conditions at neap tides result in a vertical stratification of salinity, and the resultant baroclinic circulation allows the hypersaline water to escape along the seabed (Nunes Vaz et al., 1990). During spring tides, however, the hypersaline water is trapped in Spencer Gulf due to increased tidal mixing ensuring vertical homogeneity and thus preventing a baroclinic circulation to develop. In the GBR different dynamics prevail because the bays are much more open and as a result hypersaline water is exported sideways from bay to bay by a longshore currents as well as cross-shelf by tidal diffusion. This generates a longshore gradient in the hypersalinity. The width of the hypersaline zone in coastal waters is determined by cross-shelf diffusion and the longshore export of hypersaline waters is mainly controlled by advection by the southward residual current due the Coral Sea inflow.

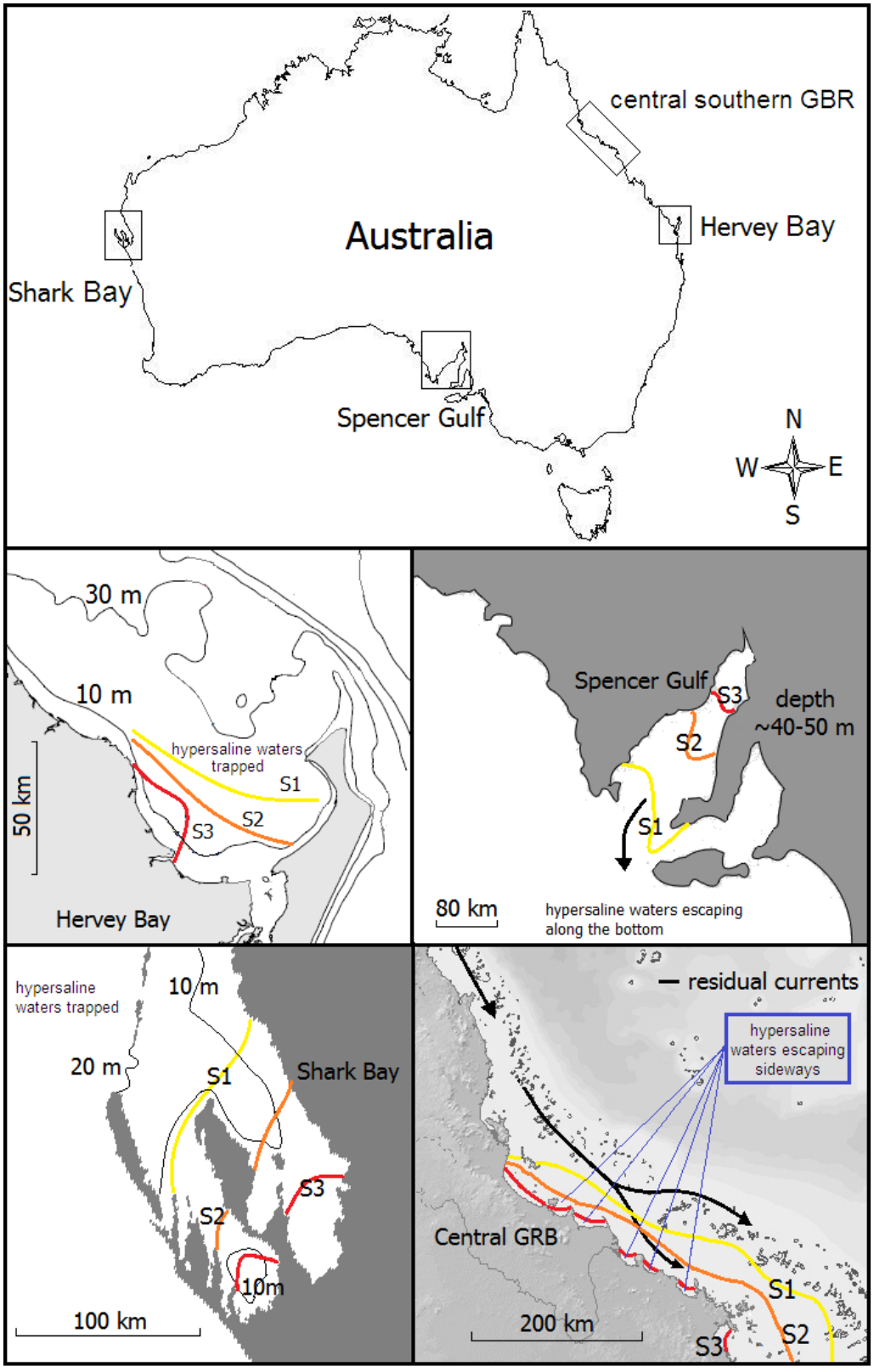

Figure 5 – Comparison between hypersalinity systems in Australia. In Spencer Gulf the hypersaline waters may be flushed out along the seabed at neap tides by salinity-driven baroclinic currents. In contrast, the waters in the shallow Hervey and Shark bays are vertically

well-mixed, thus the hypersaline waters are trapped. In the shallow GBR the hypersaline waters are transferred sideways from bay to bay by the residual currents and thus forming a coastal boundary layer of hypersaline waters.

5. Conclusions

The inflow of oceanic waters from the Coral Sea, turbulent diffusion and the wind control the dynamics of the GBR hypersaline coastal waters during the dry season. Both the magnitude of the hypersalinity and the time to reach steady-state conditions were used to compare predictions and observations. The model suggests that the cross-shelf salinity gradient was more sensitive to adjustments of the residual current inflow from the Coral Sea than adjustments to the diffusion coefficient K_h. The dynamics of the hypersaline zone are also modulated by the wind and the tides.

The dynamics of the hypersaline coastal zone in the GBR appear different from those in other hypersaline systems in Australia and world-wide. Hypersaline waters in bays along the GBR coast escape sideways by the residual longshore southward currents; hypersaline waters are thus not trapped and are transferred from bay to bay. This demonstrates connectivity between bays. The width of the hypersaline coastal zone increase longshore southwards. The model suggests that steady-state conditions are reached after about 100 days, indicating a long residence time of inshore waters. All these findings may have biological implications that need to be investigated.

6. Acknowledgements

This study was made possible by the IPRS PhD fellowship to FPA. The kind assistance of J. Lambrechts in the use of the SLIM model is gratefully acknowledged.

References

Andrews, J. C., Clegg, S., 1989. Coral Sea circulation and transport from modal information models. Deep-Sea Research, 36, 957-974.

Andrews, J. C., Bode, L., 1988. The tides of the Central Great Barrier Reef. Continental Shelf Research 8, 1057-1085.

Andrews, J. C., 1983. Water masses, nutrient levels and seasonal drift on the Outer Central Queensland Shelf (Great Barrier Reef). Australian Journal of Marine and Freshwater Research 33, 717-722.

Brandon, D. E., 1973. Waters of the Great Barrier Reef province. In: O. A. Jones and R. Endean (Eds.), Biology and Geology of Coral Reefs vol. 1, Geology 1, 187-232, Academic Press, New York.

Bray, N. A., Rubles, J. M., 1991. Physical oceanography of the Gulf of California. In: J. P. Dauphin and B. R. T. Simoneit (Eds.), The Gulf and Peninsular Province of the Californias. AAPG Mem. 47, 511-533.

Brinkman, R., Wolanski, E., Deleersnijder, E, McAllister, F., Skirving, W., 2002. Oceanic inflow from the Coral Sea into the Great Barrier Reef. Estuarine, Coastal and Shelf Science 54, 655-668.

Chadwick, D. B., Largier, J.L., 1999. Tidal exchange at the bay-ocean boundary. Journal of Geophysical Research 104 (C12), 29901-29924.

Church, J. A., Andrews, J. C., Boland, F. M., 1985. Tidal currents in the central Great Barrier Reef. Continental Shelf Research 4, 515-531.

de Brauwere, A., de Brye, B., Blaise, S., Deleersniider, E., 2011. Residence time, exposure time and connectivity in the Scheldt Estuary. Journal of Marine Systems 84, 85-95.

Diop, E. S., Soumare, A., Diallo, N., Guisse, A., 1997. Recent change of mangroves of the Saloum River Estuary, Senegal. Mangroves and Salt Marshes 1, 163-172.

Ganachaud, A., Kessler, W., Wijffels, S., Ridgway, K, Cai, W., Holbrook, N., Bowen, M., Sutton, P., Qiu, B., Timmermann, A., Roemmich, D., Sprintall, J., Cravatte, S., Gourdeau, L., Aung, T., 2007. Southwest Pacific Ocean Circulation and Climate Experiment. Part I. Scientific Background. NOAA OAR Special Report / International CLIVAR Project Office. C. P. S. N. 111.

Gutierrez de Velasco, G., Winant, C. D., 2004. Wind- and density-driven circulation in a well mixed inverse estuary. Journal of Physical Oceanography 34, 1103-1116.

King, B. A., Wolanski, E., 1996. Tidal current variability in the Central Great Barrier Reef. Journal of Marine Systems 9,187-202.

Lacombe, H., Richez, C., 1982. The regime of the Strait of Gibraltar. Elsevier Oceanography Series 34, 13-73.

Lambrechts, J., Harnet, E., Deleersnijder, E., Bernard, P. E., Legat, V., Remacle, J. F., Wolanki, E., 2008. A multi-scale model of the hydrodynamics of the whole Great Barrier Reef. Estuarine, Coastal and Shelf Science 79, 143-151.

Largier, J. L., Hollibaugh, J. T., Smith, S. V., 1997. Seasonally hypersaline estuaries in Mediterranean-climate regions. Estuarine, Coastal and Shelf Science 45, 789-797.

Lavin, M. F., Godinez, V. M., Alvarez, L. G., 1998. Inverse-estuarine features of the Upper Gulf of California. Estuarine, Coastal and Shelf Science 47, 769-795.

Lennon, G. W., Bowers, D., Nunes, R. A., Scott, B. D., Ali, M., Boyle, J., Wenju C., Herzfeld, M., Johansson, G., Nield, S., Petrusevics, P., Stephenson, P., Suskin, A. A., Wuffels, S. E. A., 1987. Gravity currents and the release of salt from an inverse estuary. Nature 327, 695-697.

Luick, J. L., Mason, L., Hardy, T., Furnas, M. J., 2007. Circulation in the Great Barrier Reef Lagoon using numerical tracers and in situ data. Continental Shelf Research 27, 757-778.

Nahas, E. L., Pattiaratchi, C. B., Ivey, G. N., 2005. Dynamics of frontal systems in Shark Bay, Western Australia. Estuarine and Coastal Shelf Science 65, 463-474.

Nunes Vaz, R. A., Lennon, G. W., Bowers, D. G., 1990. Physical behaviour of a large, negative or inverse estuary. Continental Shelf Research 10, 277-304.

Okubo, A., 1971. Diffusion diagrams. Deep-Sea Research 18, 789-802.

Orr, A. P., 1933. Physical and chemical conditions in the sea in the neighbourhood of the Great Barrier Reef.In: Scientific Report, Great Barrier Reef Expedition 1928-29 vol. II(3), 37-86, British Museum (Natural History), London.

Phillips, O. M., 1966. On the turbulent convection currents and the circulation in the Red Sea. Deep-Sea Research 13, 1149-1160.

Pickard, G. L., 1977. A Review of the Physical Oceanography of the Great Barrier Reef and Western Coral Sea. AIMS Monography Series vol. 2, Australian Government Printer, Camberra.

Ribbe, J., 2006. A study into the export of saline water from Hervey Bay, Australia. Estuarine, Coastal and Shelf Science 66, 550-558.

Sheaves, M., 2006. Scale-dependent variation in composition of fish fauna among sandy tropical estuarine embayments. Marine Ecology Progress Series 310, 173-184.

Spagnol, S., Wolanski, E., Deleersnjider, E., 2001. Steering by coral reef assemblages. In Wolanski, E. (Ed), Oceanographic Processes of Coral Reefs: Physical and Biological Links in the Great Barrier Reef. CRC Press, Boca Raton, Florida, pp. 145-160.

Valle-Levinson, A., Delgado, J. A., Atkinson, L. P., 2001. Reversing water exchange patterns at the entrance to a semiarid coastal lagoon. Estuarine, Coastal and Shelf Science 53, 825-838.

Vethamony, P., Babu, M., Ramanamurty, M., Saran, A., Joseph, A., Sudheesh, K., Padgaonkar, R., Jayakumar, S., 2007. Thermohaline structure of an inverse estuary: the Gulf of Kachchh: measurements and model simulations. Marine Pollution Bulletin 54, 697-707.

Wang, Y., Ridd, P. V., Heron, M. L., Stieglitz, T. C., Orpin, A. R., 2007. Residence time of solutes and pollutants in the central Great Barrier Reef lagoon, Australia. Marine and Freshwater Research 58,778-791.

Walker, T., 1981. Seasonal salinity variations in Cleveland Bay, Northern Queensland. Australian Journal of Marine and Freshwater Research 32, 143-149.

Walker,T., 1982. Lack of evidence for evaporation-driven circulation in the Great Barrier Reef Lagoon. Australian Journal of Marine and Freshwater Research 33, 717-722.

Webster, M. A., Petkovic, P., 2005. Australian Bathymetry and Topography Grid, June 2005. Record 2005/12.

Webster, I. T., 2010. The hydrodynamics and salinity regime of a coastal lagoon – The Coorong Australia – Seasonal to multi-decadal timescales. Estuarine Coastal and Shelf Science 90, 264-274.

Winant, C. D. and de Velasco, G. G., 2011. Dynamics of hypersaline estuaries: Laguna San Ignacio, Mexico. Chapter 12 in Volume 2: Water and fine sediment circulation, (eds., R.J. Uncles and S.G. Monismith) in the Treatise on Estuarine and Coastal Science (Series eds., E. Wolanski, and D. McLusky), Elsevier. In press.

Wolanski, E., Jones, M., 1979. Biological, chemical and physical observations in inshore waters of the Great Barrier Reef, North Queensland, 1979. Australian Institute of Marine Science, Data Report, Oceanography Series No.2.

Wolanski, E., Jones, M., Williams, W. T., 1981. Physical properties of Great Barrier Reef lagoon waters near Townsville. II Seasonal variations. Australian Journal of Marine and Freshwater Research 32, 321-34.

Wolanski, E., Pickard, G. L., Jupp, D. L. B., 1984. River plumes, coral reefs and mixing in the Gulf of Papua and the northern Great Barrier Reef. Estuarine Coastal and Shelf Science 18, 291-314.

Wolanski, E., Pickard, G. L., 1985. Long-term observations of currents on the central Great Barrier Reef continental shelf. Coral Reefs 4, 47-57.

Wolanski, E., 1986. An evaporation-driven salinity maximum zone in Australian tropical estuaries. Estuarine Coastal Shelf Science 22, 415-24.

Wolanski, E., Burrage, D., King, B., 1989. Trapping and dispersion of coral eggs around Bowden Reef, Great Barrier Reef, following mass coral spawning. Continental Shelf Research 9, 479-496.

Wolanski, E., Ridd, P., 1990. Mixing and trapping in Australian tropical coastal waters. pp. 165-183 in Cheng, R.T. (Editor), Residual Currents and Long-term Transport, Coastal and Estuarine Studies vol. 38, Springer-Verlag, New York.

Wolanski, E., 1994. Physical oceanographic processes of the Great Barrier Reef. CRC Press, Boca Raton, Florida, 194 pp.

Wolanski, E., Asaeda, T., Tanaka, A., Deleersnijder, E., 1996. Three-dimensional island wakes in the field, laboratory and numerical models. Continental Shelf Research 16, 1437-1452.